Indian Journal of Pure & Applied Physics
Vol. 61, November 2023, pp. 906-909
DOI: 10.56042/ijpap.v61i11.3463

Study on Structural and Dielectric Properties of (Ti, Cr) co-doped SnO_2 Nanoparticles

Sangeeta[a,b*], Anju Dutt[a,b], Harpreet Singh[a,b], Anand Kumar[a] & Amit Kumar[b]

[a]Department of Physics, Institute of Integrated and Honors Studies, Kurukshetra University, Kurukshetra, Haryana 136 119, India

[b]Department of Physics, Kurukshetra University, Kurukshetra, Haryana 136 119, India

Received 7 July 2023; accepted 14 August 2023

The present study deals with the impact of (Ti, Cr) co-doping on the structural, optical, and dielectric properties of the SnO_2 nanoparticles. The traditional solid-state reaction route is adopted to prepare undoped, Ti-doped and (Ti, Cr) co-doped SnO_2 nanoparticles. The structural analysis revealed the polycrystalline nature with a single phase of tetragonal rutile type structure for all the prepared samples. The increment in the crystallite size is observed with doping. The Scanning electron microscopy showed that the nanoparticles are spherical and uniformly distributed. A small variation is noticed in the optical band gap energy of doped samples as compared to the undoped SnO_2. The significant changes have been reported in parameters such as dielectric function, capacitance, dielectric loss factor, and AC conductivity. Maxwell-Wagner model is suitable to illustrate the decreasing behaviour of dielectric constant and dielectric loss with frequency. Ti and Cr co-doped SnO_2 nanoparticles revealed lower dielectric loss contrary to Ti-doped and undoped SnO_2 nanoparticles. The ac conductivity of all the prepared samples increases with frequency and doping. Ti-doped SnO_2 nanoparticles exhibited higher ac conductivity, which can be explained by the hopping of charge carriers.

Keywords: Co-doping; Structural analysis; Crystallite size; Maxwell-wagner model; Dielectric constant

1 Introduction

The metal oxide semiconductors, tin oxide (SnO_2) is n-type wide band gap semiconductor with the band gap of 3.6 eV at 300 K. SnO_2 is a riveting material for research due to its high charge carrier density, high thermal and chemical stability, high transparency in the visible region, etc. It has many advantageous applications in solar cells, gas sensors, Li-ion batteries, energy storage devices, optoelectronic devices, *etc.*[1]. The doping of transition metals, non-metals and rare earth metals can lead the tunability of chemical and physical properties of materials. Several research groups have already studied the effect of single dopants[2-6]. The combinations of co-dopants such as (Fe, Co), (Ni, Co) and (Cu, Fe) co-doped SnO_2 nanoparticles have been investigated for their structural, optical, and electrical properties[7]. As the co-doping is playing the significant role for the improvement of their properties, which motivates the researchers for the further analysis of co-dopants effects. Hence, the present study focused the structural, optical and dielectric behaviour of (Ti, Cr) co-doped SnO_2 nanoparticles. The solid-state reaction method is preferred here due to its easy processing, handling, non-pollute nature and large-scale production.

2 Synthesis and Characterization

SnO_2, $Sn_{0.985}Ti_{0.015}O_2$, $Sn_{0.97}Ti_{0.015}Cr_{0.015}O_2$, $Sn_{0.95}Ti_{0.015}Cr_{0.035}O_2$ and $Sn_{0.93}Ti_{0.015}Cr_{0.055}O_2$ were prepared using solid-state reaction route. The samples were marked as C0, C1, C2, C3, and C4, respectively, for simplicity. The SnO_2, TiO_2, and Cr_2O_3 powders with high purity (99.99 %) were used as the starting materials. All the materials were mixed in the stoichiometric ratio and grounded for 6 hours with acetone. The obtained mixture was annealed at 900 °C for 6 hours and grounded again for 3 hours. To get a homogenous mixture, the mixture was again annealed at 900 °C for 3 hours. Obtained mixture was used to prepare the pellets of 13mm diameter and 2mm thickness by the hydraulic press under a pressure of 70 Kg/cm^2. The pellets were sintered at 1100 °C for 5 hours with a heating rate of 5°/min. For the phase analysis, the samples were characterized by X-ray diffractometer (D8 advance, BRUKER) with Cu-Kα radiation (λ = 1.5406 Å) in 2θ range from 20°–80° and 0.02 step size. The Rietveld refinement was performed using FullProf software to extract the

*Corresponding author:
(E-mail: sangeeta@kuk.ac.in)

accurate structural parameters and to confirm the phase of the prepared samples. The surface morphology was investigated by using the field emission scanning electron microscope (FESEM, 7610F Plus/JEOL) combined with energy dispersive spectroscopy (EDS). To examine the optical properties, the UV-visible spectroscopy (Shimadzu UV 3600 plus UV-VIS-NIR) was used in the wavelength range of 200–800 nm. The dielectric measurements were carried out by using a high-precision impedance analyzer (Wayne Kerr 6500B) in the frequency range from 100 Hz to 1 MHz at room temperature.

3 Result and Discussion

The XRD patterns of C0, C1, C2, C3, and C4 nanoparticles are illustrated in Fig. 1(a). All the diffraction peaks of crystal planes are perfectly matched with the rutile type tetragonal structure of SnO_2 (JCPDS/ICCD no. 41-1445)[8]. No impurities are observed within the sensitivity limit of the X-ray diffractometer which confirm the single phase of all the prepared samples. Fig. 2 illustrates the refinement patterns of all the prepared samples, the experimental and observed peaks are well fitted[9]. The values of lattice parameters of C1, C2, C3, and C4 are smaller than C0 (Table 1) which are attributed to the smaller ionic radii of Ti^{4+} (0.61Å) and Cr^{3+} (0.62Å) than Sn^{4+} (0.69Å). The variation of lattice parameters and cell volume with dopants concentration refers to the substitution of dopants into the host lattice without any change in its crystal structure[10]. The evolution of the intensity and shifting of the peak as shown in Fig. 1(b) corresponding to (110) plane also indicates the successful incorporation of both dopants into the SnO_2 lattice. The co-doping enhances the crystallinity of the pure SnO_2. Both dopants carry the half value of atomic scattering factor compared to SnO_2 which ultimately changes the structure factor and results in higher intensity. The evolution of XRD peaks is also observed by other researchers with the substitution of dopants in SnO_2 matrix[11-12].

The average crystallite size of all the prepared samples is calculated by using Debye Scherrer's formula

$$D = \frac{k\lambda}{\beta Cos\theta} \quad \ldots (1)$$

Where, D is the average crystallite size, K is constant having value 0.9, λ is wavelength, β is FWHM and θ is the diffraction angle.

The surface morphology of all the prepared samples is analyzed by using the SEM technique. Fig. 3(a-e) shown the SEM images of all prepared samples. It is clear from the figure that the particles

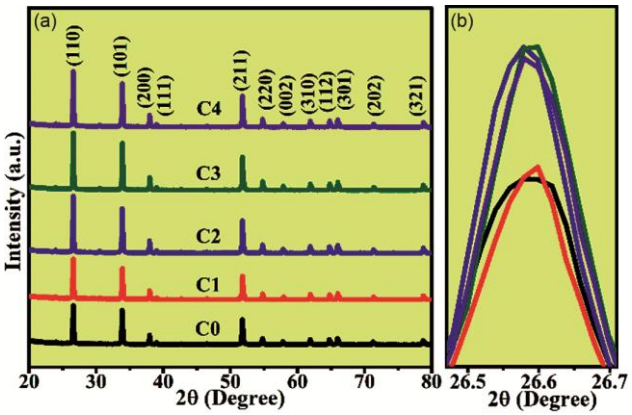

Fig. 1 — XRD patterns of all prepared samples.

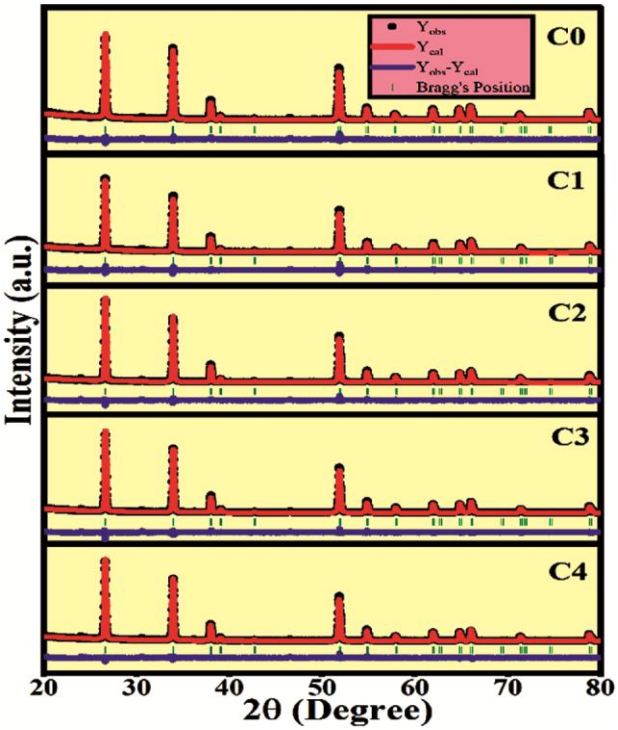

Fig. 2 — Rietveld refinement of all prepared samples.

Table 1 — The structural parameters of all prepared pristine and doped SnO_2 samples

Sample	a = b (Å)	c (Å)	V (Å^3)	Crystallite size (nm)
C0	4.7366	3.1845	71.45	38.58
C1	4.7362	3.1820	71.38	42.41
C2	4.7372	3.1830	71.43	43.88
C3	4.7348	3.1820	71.33	44.19
C4	4.7354	3.1822	71.36	43.49

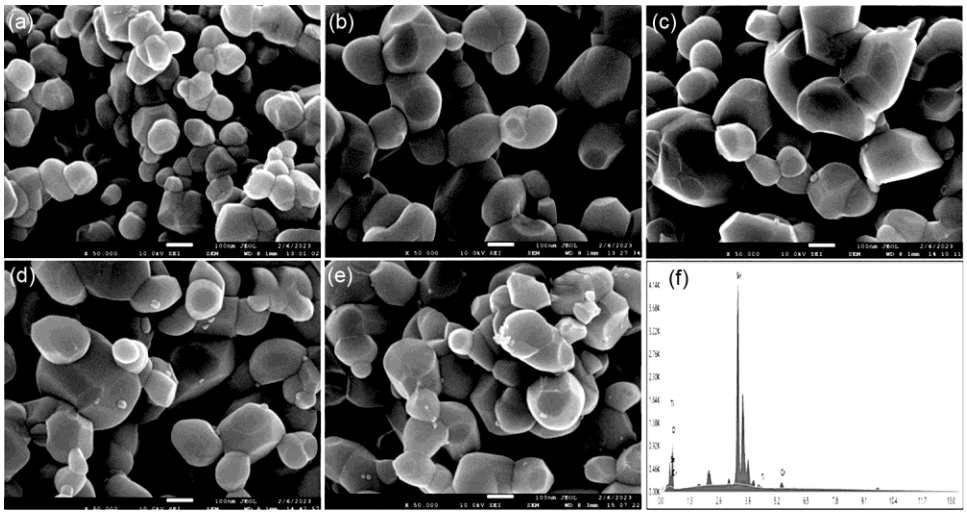

Fig. 3 — SEM images of (a) C0, (b) C1, (c) C2, (d) C3, (e) C4 and (f) EDS spectra of C4.

are homogeneous, spherical in shape, and uniformly distributed. The average grain size is calculated by using image J software. The values of average grain size are found to be 81 nm, 95 nm, 102 nm, 104 nm and 98 nm for C0, C1, C2, C3, and C4, respectively. The energy dispersive spectroscopy (EDS) shown in Fig. 3 (f) confirms the presence of Sn, O, Ti and Cr in the synthesized samples. The absence of extra phase in the SnO_2 lattice in XRD patterns substantiated by the EDS spectra.

The optical band gap is determined by using Tauc's equation,[13]

$$\alpha h\nu = A\,(h\nu - E_g)^{1/2} \qquad \ldots (2)$$

Where, α, h, ν, A and E_g are the absorption coefficient, Planck's constant, photon frequency, absorption constant, and optical band gap, respectively. The optical band gap is obtained by extrapolating the linear region of plot $(\alpha h\nu)^2$ *vs.* $h\nu$ and setting the $(\alpha h\nu)^2$ scale to zero. The absorption spectra and the Tauc's plots of C0, C1, C2, C3 and C4 are described in Fig. 4. The depletion of the optical band gap might be due to sp-d exchange interaction between the band electrons and localized d-electrons of Ti^{4+} and Cr^{3+} ions substituting at place of Sn^{4+}. The s-d and p-d exchange interactions engender the negative and positive corrections to the conduction band and valance band edges, respectively, resulting in band gap narrowing[14]. However, the increasing value of the band gap of C3 and C4 is ascribed to the shifting of the fermi level towards the conduction band. This shifting is caused by the enhancement of the carrier density of dopants which increases the band gap and is attributed to the Burstein-Moss effect[15].

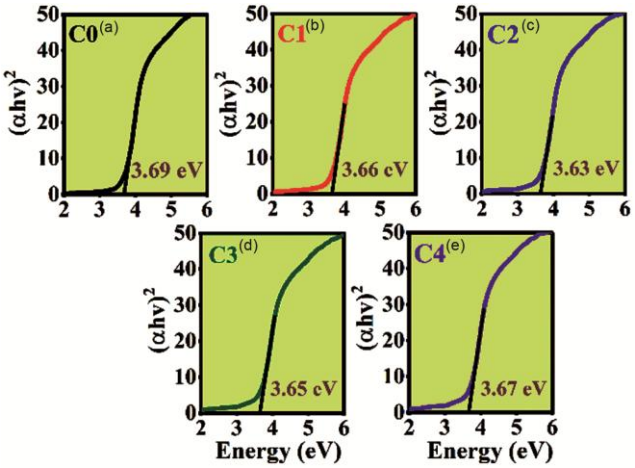

Fig. 4 — Tauc's plots of all prepared samples.

Generally, the complex dielectric constant can be written as,

$$\varepsilon * = \varepsilon' + i\varepsilon'' \qquad \ldots (3)$$

where, $\varepsilon'$and ε'' are the real and imaginary parts of the dielectric constant associated with the stored energy and dissipated energy of the medium, respectively. The dielectric constants can be calculated by using the relation (4) and (5).

$$\varepsilon' = \frac{Cd}{\varepsilon_0 A} \qquad \ldots (4)$$

and

$$\varepsilon'' = \varepsilon' \tan\delta \qquad \ldots (5)$$

where, C, d, A, $\tan\delta$ and ε_0 are the capacitance of the material, thickness of the pellet, area of the cross-section of the pellet, dielectric loss, and the permittivity of free space (8.854×10^{-12} F/m) [16].

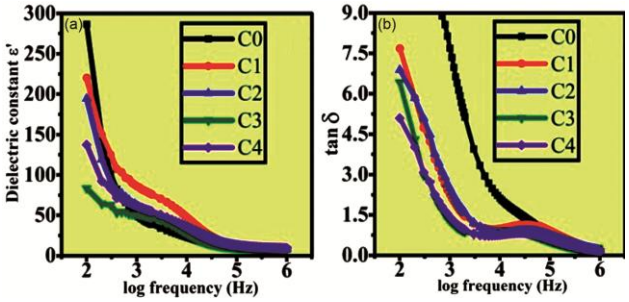

Fig. 5 — (a) variation of dielectric constant and (b) dielectric loss (tanδ) with frequency.

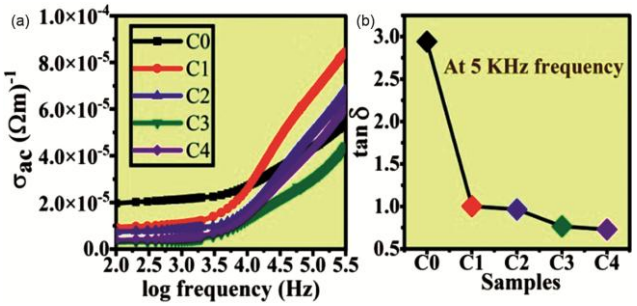

Fig. 6 — (a) variation of ac conductivity with frequency and (b) tanδ loss of all prepared samples at 5 KHz.

The dielectric behavior is depicted in Fig. 5 (a,b) and can be explained on the basis of Maxwell-Wagner model[7]. When a current flows across the interface, charges are accumulated at the boundaries followed by space charge or interfacial polarization. Here, the large polarization and high dielectric constant at lower frequencies are observed. At higher frequencies, the interfacial polarization gets diminished as the dipoles are unable to alter their direction promptly and lags behind the electric field. The probability of charge carriers moving towards grain boundaries goes down which ultimately decreases the polarization and the dielectric constant becomes almost constant with higher frequency[9]. The dielectric constant decreases with co-dopants which might be due to the dissimilarities of ionic radii of Sn^{4+}, $Ti^{4+,}$ and Cr^{3+} ions and the substitution of dopants at the site of Sn[17].

The dielectric loss factor (tanδ) shows the same behavior as the dielectric constant. Due to free charge carriers development, the tanδ decreases with increasing dopant concentration and frequency (Fig. 5 (b) & 6 (b)). The ac conductivity increases with frequency, but the co-doping discourages the ac conductivity as mentioned in Fig. 6(a). This behaviour can be explained by the hopping model [18].

4 Conclusion

Both dopants are successfully incorporated into the SnO_2 matrix by adopting solid-state reaction method. Rietveld refinement plots confirm the single-phase rutile type structure for all prepared samples. Average crystallite sizes are found in the range 39 nm - 44 nm.

The significant changes have been observed in the dielectric behavior of doped and co-doped samples. The dielectric loss factor (tanδ) value 2.9 is observed for pure SnO_2 (C0) and this value gradually decrease to 0.7 for highly doped SnO_2 (C4) sample. The diminished value of dielectric loss implies the highest amount of stored energy. So, the results are useful for energy storage devices.

Acknowledgement

The authors Sangeeta/HS acknowledge Council of Scientific & Industrial Research (CSIR), New Delhi (India)/ University Grant Commission (UGC), New Delhi (India) for financial support in terms of Senior Research Fellowship. Sangeeta also acknowledges Ion Beam Centre, K.U.K. for providing the facility of XRD and UV-Visible - NIR spectroscopy.

References

1 Snaith H J & Ducati C, *Nano Lett*, 10 (2010) 1259.
2 Azam A, et al., *J Alloys Compd*, 506 (2010). 237.
3 Pandian S K, et al., *Mater Manuf Process*, 27 (2012) 130.
4 Tagreed M, et al., *Energy Procedia*, 157 (2019) 457.
5 Ahmed A, et al., *Mater Sci Eng*, 577 (2019) 012041.
6 Jahnavi V S, et al., *J Electron Mater*, 49 (2020) 3540.
7 Mehraj S & Ansari M S, *Phys. E Low-dimensional Syst Nanostruct*, 65 (2015) 84.
8 Wan N, et al., *Scientific Reports*, 6 (2016) 1.
9 Narzary R, et al., *Mater Sci Semicond Process*, 142 (2022) 106477.
10 Duhan M, et al., *Vacuum*, 181 (2020) 109635.
11 Gopinadhan K, et al., *J Appl Phys*, 102 (2007) 113513.
12 Kuppan M, et al., *Adv Condens Matter Phys*, 2014 *(2014)*.
13 Ahmed A, et al., *Appl Surf Sci*, 483 (2019) 463.
14 Subramanyam K, et al., *Solid State Sci*, 39 (2015) 74.
15 Lachore W L, et al., *Appl Phys A*, 128 (2022) 515.
16 Ahmed R, et al., *Mater Res Bull*, 63 (2015) 32.
17 Rajwali K & Fang M H, *Chin Phys B*, 24 (2015) 127803.
18 Sahay P P, et al., *Curr Appl Phys*, 13 (2013) 479.